

# Geophysical Research Letters

## RESEARCH LETTER

10.1029/2019GL084198

### Key Points:

- MMS observed interstellar pickup He<sup>+</sup> upstream and downstream of the Earth's perpendicular bow shock
- Comparison of upstream and downstream velocity distributions revealed accelerated pickup He<sup>+</sup>
- The observations are consistent with single reflection shock acceleration

### Correspondence to:

M. J. Starkey,  
ayj611@my.utsa.edu

### Citation:

Starkey, M. J., Fuselier, S. A., Desai, M. I., Burch, J. L., Gomez, R. G., Mukherjee, J., et al. (2019). Acceleration of interstellar pickup He<sup>+</sup> at Earth's perpendicular bow shock. *Geophysical Research Letters*, 46, 10,735–10,743. <https://doi.org/10.1029/2019GL084198>

Received 21 JUN 2019

Accepted 3 SEP 2019

Accepted article online 6 SEP 2019

Published online 16 OCT 2019

## Acceleration of Interstellar Pickup He<sup>+</sup> at Earth's Perpendicular Bow Shock

M. J. Starkey<sup>1,2</sup> , S. A. Fuselier<sup>1,2</sup> , M. I. Desai<sup>1,2</sup>, J. L. Burch<sup>2</sup> , R. G. Gomez<sup>2</sup>, J. Mukherjee<sup>2</sup> , C. T. Russell<sup>3</sup> , H. Lai<sup>3</sup>, and S. J. Schwartz<sup>4</sup> 

<sup>1</sup>Physics and Astronomy, University of Texas at San Antonio, San Antonio, TX, USA, <sup>2</sup>Southwest Research Institute, San Antonio, TX, USA, <sup>3</sup>Earth, Planetary, and Space Sciences, University of California, Los Angeles, CA, USA, <sup>4</sup>Laboratory for Atmospheric and Space Physics, University of Colorado Boulder, Boulder, CO, USA

**Abstract** On 05 December 2015 the Magnetospheric MultiScale constellation observed interstellar pickup ion distributions during an inbound crossing of Earth's perpendicular bow shock near the subsolar point, which provides new insights into shock acceleration of pickup ions throughout the heliosphere. In this study we analyze the upstream and downstream velocity distributions of H<sup>+</sup> and He<sup>+</sup> using data from the Hot Plasma Composition Analyzer on Magnetospheric MultiScale. We derive average two-dimensional pitch angle distributions in the upstream and downstream field-aligned bulk plasma frame, as well as integrated one-dimensional velocity distributions. By comparing the upstream and downstream distributions, we find evidence of accelerated H<sup>+</sup> and He<sup>+</sup> downstream of the shock. By comparing measured and theoretical reflection ratios for He<sup>+</sup>, we attribute a significant part of this acceleration to a single reflection at the shock.

**Plain Language Summary** By studying distributions of ions before and after a shock in space, we gain valuable insights into shock acceleration mechanisms that produce high-energy ion populations, observed throughout the heliosphere. On 05 December 2015 the Magnetospheric MultiScale constellation crossed Earth's perpendicular bow shock and measured velocity distributions of He<sup>+</sup> ions before and after the shock. This study analyzes these distributions in search for signs of accelerated He<sup>+</sup>. We find that He<sup>+</sup> is accelerated mainly perpendicular to the local magnetic field, and that a significant fraction of the accelerated He<sup>+</sup> is consistent with the theory of shock reflection at the bow shock, in which an ion is reflected at the shock and then energized by the solar wind electric field (pointing parallel to the shock surface) as the ion gyrates back to the shock.

## 1. Introduction

As the heliosphere moves through the local interstellar medium, neutral particles are ionized via charge exchange or photoionization. These freshly ionized particles, called interstellar pickup ions (PUI), move with speed  $|\vec{V}_{SW} - \vec{V}_{LISM}|$ , relative to the solar wind. Here  $\vec{V}_{SW}$  is the solar wind bulk velocity and  $\vec{V}_{LISM}$  is the relative velocity of the local interstellar medium and the heliosphere. The relative velocity of the interstellar neutral flow to the heliosphere has been extensively studied using PUI observations (Gloeckler, Möbius, et al., 2004), neutral atoms (McComas et al., 2015; Witte, 2004), and UV backscattering (Vallerga et al., 2004). Currently,  $V_{LISM}$  is estimated to be  $\sim$ 26.24 km/s (Möbius et al., 2004). This is small compared to typical solar wind velocities ( $V_{SW} \sim$ 400 km/s); thus, we neglect  $V_{LISM}$  in this paper and assume that fresh PUIs move with  $V_{SW}$ . A fresh PUI will gyrate perpendicular to the local interplanetary magnetic field (IMF) with speed  $\leq V_{SW}$  in the solar wind rest frame. The resulting PUI velocity in the solar wind frame consists of two components: (1) gyromotion perpendicular to the local IMF and (2) guiding center motion parallel to the local IMF. Thus, velocity distribution functions (VDF) of fresh PUIs are initially assumed to resemble a torus distribution, with radius  $\sim V_{SW}$ . Work by Vasylunas and Siscoe (1976) suggested that the PUI torus adiabatically evolves into an isotropic shell distribution due to resonant wave-particle interactions, while cooling adiabatically due to the radially expanding solar wind. We note, however, that studies by Gloeckler et al. (1995) and Möbius et al. (1998) observed PUI distributions with anisotropic features. To date, there have been multiple observations of PUI distributions (Drews et al., 2013; Drews et al., 2015; Gloeckler & Geiss, 1998; Gloeckler, Geiss, et al., 2004; Möbius, et al., 2004; Gomez et al., 2019; McComas et al., 2017; Möbius & Hovestadt, 1985). With PUIs readily detectable, it is possible to study the evolution of PUI populations throughout the solar

wind. Singly charged PUIs, with speed  $2V_{SW}$  and mass  $m$ , will have energies larger than that of bulk solar wind protons by a factor of  $4m/m_p$ , where  $m_p$  is the proton mass. Therefore, PUIs have significantly higher speeds relative to bulk solar wind ions, suggesting that PUIs are an important source of seed particles for acceleration.

It is largely agreed upon that ions can be accelerated at shocks in space, such as CME shocks, CIR shocks, planetary bow shocks, and the termination shock. In particular, for quasi-perpendicular shocks, where the angle between the local IMF,  $\vec{B}_{IMF}$ , and the shock normal,  $\vec{n}_{sh}$ , is greater than  $45^\circ$ , observations of accelerated downstream ions have been attributed to shock drift acceleration and specular shock reflection (Sckopke, 1995; Sckopke & Paschmann, 1983; Sckopke et al., 1990; Sonnerup, 1969). In the theory of shock reflection, an ion incident at a quasi-perpendicular shock will reflect if the ion's normal incident velocity (relative to the shock) is not large enough to overcome the electrostatic shock potential in the normal incidence frame (NIF; Auer, 1971; Leroy et al., 1981). The shock potential energy is estimated as the difference between the upstream and downstream energy of a proton moving with the bulk flow speed. A reflected ion gyrates through the upstream and back to the shock, gaining energy in the solar wind electric field,  $\vec{E}_{SW} = -\vec{V}_{SW} \times \vec{B}_{IMF}$ . There has been observational evidence for PUI acceleration at different types of quasi-perpendicular shocks (Gloeckler et al., 1994; Gloeckler, Geiss, et al., 2004; Oka et al., 2002; Zank et al., 1996; Zirnstein et al., 2018), as well as simulation and theoretical work regarding PUI acceleration at quasi-perpendicular shocks and the termination shock (Ellison et al., 1999; Giacalone & Jokipii, 1995; Kucharek & Scholer, 1995; Lee et al., 1996; Zank et al., 1996). However, aside from Oka et al. (2002) and Gloeckler et al. (1994), there is a lack of direct observations of species-resolved accelerated PUIs at quasi-perpendicular shocks.

The Magnetospheric MultiScale (MMS) mission provides ion composition and magnetic field data, which provides insights for studying PUI VDFs across shocks in space. By comparing PUI VDFs, upstream and downstream of shocks in space, one can then identify accelerated PUIs.

In this paper we compare  $\text{He}^+$  and  $\text{H}^+$  VDFs upstream and downstream of Earth's perpendicular bow shock. We observe accelerated  $\text{H}^+$  and  $\text{He}^+$  downstream of the shock by comparing upstream and downstream two-dimensional (2-D) and 1-D VDFs in the local bulk plasma frame of reference. We attribute this acceleration to reflection of ions at the bow shock, which is supported through the calculation and comparison of measured and theoretical reflection ratios for  $\text{He}^+$  ions.

## 2. Spacecraft and Observations

From the MMS suite of instruments, we use ion data from the Hot Plasma Composition Analyzer (HPCA) instrument (Young et al., 2014) and magnetic field data from the Fluxgate Magnetometer (Torbert et al., 2016), located on each of the four MMS spacecraft (Young et al., 2014). The outbound bow shock crossing analyzed in this paper occurred on 05 December 2015 at  $\sim 8:43$  UT, when the four MMS spacecraft passed from the Magnetosheath (MS) into the solar wind (SW). In the Geocentric Solar Ecliptic (GSE) coordinate system, the MMS constellation was located at roughly  $(11.68, 0.54, -1.0) R_E$ , or very near the subsolar point. This event occurred as Earth passed through the He focusing cone, which refers to the region of increased neutral particle flux due to the solar gravitational influence on interstellar neutrals flowing through the heliosphere (Möbius et al., 1985). PUI fluxes are thus substantially increased within this region, resulting in better counting statistics for  $\text{He}^+$  measurements from MMS.

In this paper, we present PUI VDFs in a field-aligned coordinate system, in the bulk plasma frame of reference, for regions upstream and downstream of Earth's quasi-perpendicular bow shock. Figure 1 shows time series survey data from MMS3 of the shock-crossing event, including the upstream and downstream (SW and MS) time intervals used to create VDFs in our analysis. From top to bottom (Figures 1a–1f), this figure shows  $\text{H}^+$  and  $\text{He}^+$  omnidirectional differential energy intensity for an ion of energy/charge values up to 10 keV, followed by the magnitude ( $|\vec{B}|$ ), clock angle ( $\varphi = \tan^{-1}\left(\frac{B_y,GSE}{B_z,GSE}\right)$ ), and cone angle ( $\theta = \cos^{-1}\left(\frac{B_x,GSE}{|\vec{B}|}\right)$ ) of the IMF. Lastly, the bottom panel shows the three  $\text{H}^+$  bulk velocity components,

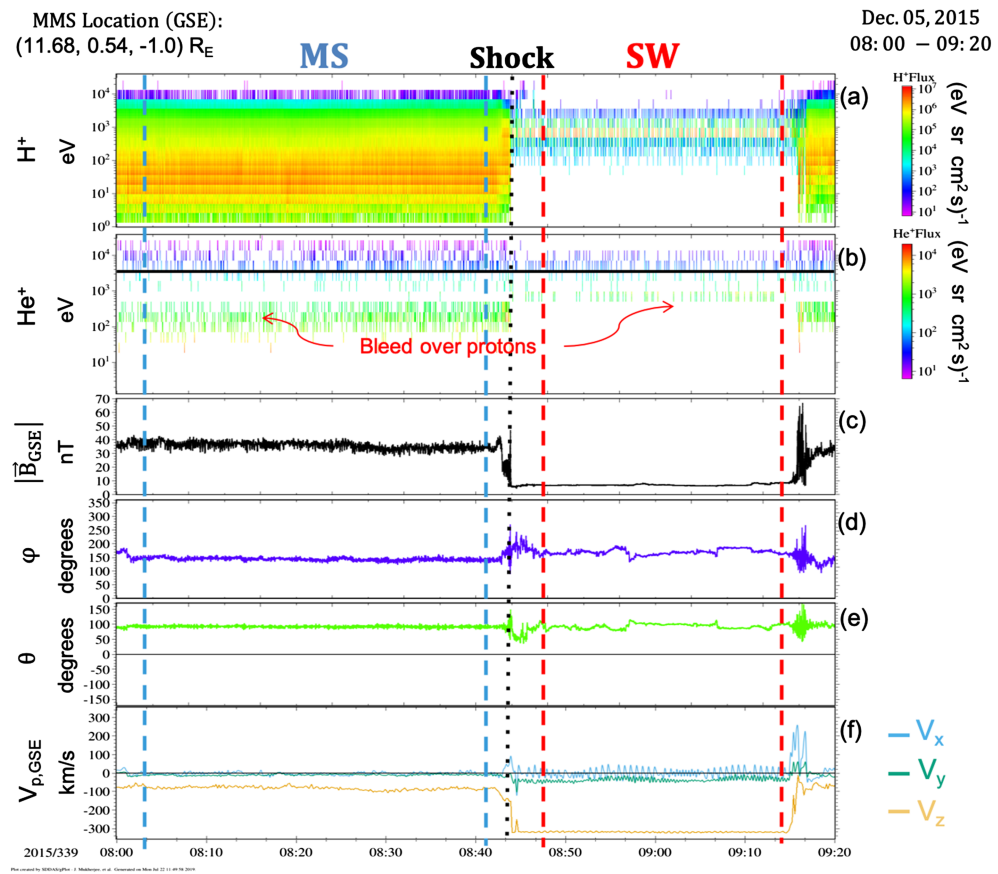


**Figure 1.** Overview plot of the bow shock crossing by MMS3 on 05 December 2015. The dotted black line indicates the shock, while the blue and red dotted lines indicate the MS interval (08:03–08:41 UT) and SW interval (08:47–09:13 UT). (a and b) The H<sup>+</sup> and He<sup>+</sup> omnidirectional differential intensity. The solid black horizontal line in (b) indicates energy step 47 (3,173.78 eV), which is used as the upper energy threshold to remove solar wind influence from the He<sup>+</sup> distributions. (c–e) The magnetic field strength, clock angle, and cone angle of the IMF in GSE. (f) Three proton bulk velocity components in GSE.

in GSE coordinates. The pair of blue lines indicate the MS time interval (08:03–08:41 UT) and the red lines indicate the SW time interval (08:47–09:13 UT).

These intervals were chosen to maximize the observation time in the relatively calm MS and SW regions, and in particular the relatively constant IMF direction. The region of weak  $B$  field and fast bulk flow speeds characterizes the SW interval, while the MS interval contains a stronger  $B$  field and slower bulk flow speed. In the He<sup>+</sup> intensity plot (Figure 1b) there is a band near 1 keV which corresponds to the energy of bulk solar wind protons. When proton fluxes into HPCA are high and within a narrow range of energies, such as in the solar wind, uncorrelated coincidence counts are recorded in the time-of-flight (TOF) data for heavier ion species at solar wind proton energies. Thus, the band in Figure 1b at the proton solar wind energy/charge is not a true He<sup>+</sup> signal and is referred to as bleed-over protons. To isolate PUIs in our analysis, these lower solar wind energy channels are removed (discussed further in section 3).

In GSE coordinates, the shock normal was determined using ACE solar wind data as input to the Merka2005 model of Earth's bow shock (Merka et al., 2005). This gave  $\hat{n}_s = (0.99, 0.01, -0.05)$ , which agreed with the shock normal computed based on timing between the four MMS spacecraft,  $\hat{n}_s = (0.98, -0.20, 0.10)$ . The angle between the upstream magnetic field and the shock normal,  $\theta_{Bn}$ , was estimated to be  $\sim 89^\circ$  (Merka2005) and  $\sim 85^\circ$  (spacecraft timing). In this paper, we use  $\theta_{Bn} = 85^\circ$ , as computed based on four-spacecraft timing. The solar wind Alfvén Mach number was computed from ACE data to be  $\sim 6.2$  at the time of MMS bow shock crossing event (8:43 UT). The shock studied in this paper is near perpendicular.

### 3. Data Analysis

HPCA consists of a toroidal electrostatic analyzer in series with an optically coupled carbon foil TOF section, which provides measurements of a particle's energy-per-charge ( $E/q$ ) and energy-per-mass ( $E/m$ ) ratio, respectively (Young et al., 2014). HPCA ion products are used to determine VDFs for a given species ( $\text{H}^+$ ,  $\text{He}^{2+}$ ,  $\text{He}^+$ ,  $\text{O}^{2+}$ , and  $\text{O}^+$ ). In survey mode, HPCA scans the full phase space of  $E/q$  and solid angle (64 energy  $\times$  16 azimuth  $\times$  16 elevation) every 10 s. For each pixel in the  $64 \times 16 \times 16$  phase space, a velocity vector is assigned based on the electrostatic analyzer voltage setting and look angle direction of that pixel. This defines a 3-D VDF corresponding to the phase space density (psd) distribution. To observe the behavior of interstellar PUIs relative to the magnetic field, we must analyze the velocity components in the bulk plasma frame and relative to the local magnetic field. Thus, VDFs are first translated into the bulk velocity ( $\vec{V}_{\text{Bulk}}$ ) frame of reference, where  $\vec{V}_{\text{Bulk}}$  is determined from the proton VDF at a 10-s cadence. Once in this frame, VDFs are rotated to a local magnetic field-aligned coordinate system defined by

$$\hat{x} = \frac{(\hat{b} \times \vec{V}_{\text{Bulk}}) \times \hat{b}}{\|(\hat{b} \times \vec{V}_{\text{Bulk}}) \times \hat{b}\|}, \quad \hat{y} = \frac{(\hat{b} \times \vec{V}_{\text{Bulk}})}{\|(\hat{b} \times \vec{V}_{\text{Bulk}})\|}, \quad \hat{z} = \hat{b} = \frac{\vec{B}_{\text{IMF,GSE}}}{\|\vec{B}_{\text{IMF,GSE}}\|}$$

This is done for each individual energy-angle-angle measurement from HPCA, using the HPCA proton moments and the Fluxgate Magnetometer magnetic field averaged over the 10-s cadence. We next define a 2-D uniformly spaced Cartesian grid ( $40 \times 40$ -km/s bins) of  $v_{\parallel}$  versus  $V_{\perp}$  where  $v_{\parallel} = v_z$  and  $V_{\perp} = \sqrt{v_x^2 + v_y^2}$ . The average psd corresponding to a constant pitch angle,  $\alpha = \tan^{-1}(V_{\perp}/V_{\parallel})$ , is then assigned to the corresponding 2-D bin, giving a 2-D distribution defined by

$$f(V_{\parallel}, V_{\perp}) = \frac{1}{2\pi} \int_0^{2\pi} f(V_{\perp}, \varphi, V_{\parallel}) d\varphi \quad (1)$$

These 2-D distributions are computed at 10-s cadence and then time-averaged over the interval of interest. From these time-averaged distributions, we compute 1-D distributions ( $f(v_{\parallel})$ ,  $f(V_{\perp})$ , and  $f(v)$ ) defined by

$$f(V_{\parallel}) = \int_{V_{\perp}} 2\pi f(V_{\parallel}, V_{\perp}) V_{\perp} dV_{\perp} \quad (2)$$

$$f(V_{\perp}) = \int_{V_{\parallel}} 2\pi f(V_{\parallel}, V_{\perp}) V_{\perp} dV_{\parallel} \quad (3)$$

$$f(v) = \int_0^{\pi} 2\pi f(V_{\parallel}, V_{\perp}) V^2 \sin\theta d\theta, \quad (4)$$

where  $\theta = \cos^{-1}(V_{\parallel}/V)$  and  $V = \sqrt{V_{\parallel}^2 + V_{\perp}^2}$ . The integrals in equations (2)–(4) are computed for constant bin sizes in  $\theta$  of  $\frac{\pi}{8}$  rad. Each phase space contribution to an integral is the average phase space within the contributing phase space pixel. In the remainder of this paper, 1-D and 2-D distributions will refer to these interval-averaged distributions in the bulk plasma frame.

#### 3.1. Solar Wind Removal

Although singly charged  $\text{He}^+$  is the third most abundant ion in the solar wind, it makes up only a fractional percent of the total ion content (Kucharek et al., 2003). The high flux of solar wind protons results in uncorrelated coincidence counts in the TOF section of HPCA (when measuring solar wind energies), which are then recorded as counts in TOF bins corresponding to different ion species. These bleed-over protons thus present a significant background source in our  $\text{He}^+$  distributions. We first note that all four HPCAs are equipped with radio frequency (RF) capability, which significantly reduces proton fluxes into the TOF section and therefore significantly reduces the bleed-over protons. In the RF setting, an RF voltage component is added to the applied electrostatic analyzer voltage, effectively creating a low-resolution RF ion mass spectrometer as described in Burch et al. (2005). MMS1 and MMS2 are operated differently from MMS3 and MMS4. For MMS1 and MMS2, bleed-over proton flux is reduced by an average factor of 2 from about 0.5 to 1 keV and about 40% from 1 to 4 keV. For MMS3 and 4, the proton flux is reduced by an average factor

of 10 from 0.5 to 1 keV and about 40% from 1 to 4 keV. Since the spacecraft are close together (much closer than a proton gyroradius), we compare measurements from MMS1 and MMS2 with those from MMS3 and 4 to distinguish between real and false signals in our  $\text{He}^+$  distributions. During quiet solar wind conditions,  $\text{He}^+$  is typically of interstellar pickup origin with energies from less than to greater than the energies of bulk solar wind protons (Möbius et al., 1985). Thus, to isolate PUIs in our SW distributions, we removed counts from energy channels corresponding to solar wind energies ( $\sim 534$  eV for  $V_{\text{SW}} = 320$  km/s). To determine the appropriate upper energy channel, we compared 2-D  $\text{He}^+$  distributions while varying the energy channel. In HPCA survey mode, counts from every four energy steps are summed together due to telemetry constraints. Thus, we tested different energy thresholds by consecutively removing blocks of four energy channels. We looked for the block of four energy channels (represented by the highest-energy channel) for which the psd at and in the neighboring pixels to the origin was 0. We determined the appropriate energy threshold to be channel 47 (of 63 total). To account for bleed-over protons, we present spacecraft-averaged distributions from MMS3 and MMS4 only and removed energy channels 0–47 (1.35–3,173.78 eV) from all of the  $\text{He}^+$  distributions. The  $\text{H}^+$  ion distributions contain all energy channels.

#### 4. Results and Discussion

Figure 2 shows 2-D and 1-D VDFs for  $\text{H}^+$  (top) and  $\text{He}^+$  (bottom), during both the SW and MS time intervals of interest. The left two columns correspond to the SW interval, while the right two columns correspond to the MS interval. For each interval and ion species there is a 2-D VDF and a 1-D VDF. The 2-D distributions show psd as a function of perpendicular (horizontal axis) and parallel (vertical axis) velocities relative to the local IMF in the plasma rest frame. The 1-D distributions show the three reduced phase space densities,  $f(V_{\parallel})$ ,  $f(V_{\perp})$ , and  $f(V)$ , as functions of the translated and normalized velocity,  $(V - V_{\text{Bulk}})/V_{\text{SW,HPCA}}$ . Here  $V_{\text{SW,HPCA}}$  is the spacecraft average (MMS34) of the average value of the bulk velocity during the solar wind interval, from each spacecraft.

Comparing first, the 2-D SW and MS distributions of  $\text{H}^+$ , we see broadening and increases in the perpendicular and parallel directions. This indicates a combination of heating and acceleration of the ions as they move across the shock. While the bulk of the SW protons decelerate across the shock, the shock heating is related to the reflection of  $\sim 20\%$  of the incident solar wind (Sckopke et al., 1990). Work by Gloeckler et al. (1994) found that the reflection efficiency of PUIs is almost 100 times that of solar wind ions, and decreases with increasing mass/charge. The higher PUI efficiency is likely due to their shell-like distribution, compared to the Maxwellian distribution of the solar wind, as proposed by Zank et al. (1996). Due to bleed-over solar wind  $\text{H}^+$  ions causing uncorrelated coincidence counts in HPCA's TOF section (discussed in section 3.1), it is difficult to distinguish PUI  $\text{H}^+$  ions in the SW and MS intervals. The peak at  $\sim 2V_{\text{sw}}$  is likely the high-energy portion of the PUI  $\text{H}^+$  distribution, while the bulk portion of the PUI distribution is indistinguishable due to contamination by solar wind protons. Furthermore, a full comparison of reflection efficiencies between PUI species ( $\text{H}^+$ ,  $\text{He}^{++}$ , and  $\text{He}^+$ ) is beyond the scope of this paper, which is to determine the nature and amount of accelerated PUI  $\text{He}^+$ .

Next we compare SW and MS  $\text{He}^+$  distributions (second row of Figure 2). First note that since  $\text{He}^+$  is expected only as a PUI in the solar wind, any counts near solar wind energies are probably bleed-over protons. Thus, by removing solar wind energy channels, we are mostly removing false counts and our final  $\text{He}^+$  distributions should accurately represent the true  $\text{He}^+$  population. In the 2-D SW distribution, the high psd ( $\sim 10^{-25}$  s<sup>3</sup>/m<sup>6</sup>) located within the arc,  $v = V_{\text{sw}}$ , indicates a nearly uniform shell distribution in velocity space, with some thickness. The parallel  $\text{He}^+$  distribution in the MS region shows broadening for velocities  $>\sim 1.7V_{\text{sw}}$  which corresponds to phase space densities  $< 10^{-16}$ . This is  $\sim 2$  orders of magnitude lower than the peak phase space densities of  $f(V_{\perp})$ . Thus, little-to-none heating/acceleration in the parallel direction is apparent in the downstream region. Note that the lower and broader peak of the  $\text{H}^+$   $f(V_{\parallel})$  distribution in the SW region, compared to the MS region, is due to the coarseness in angular resolution of HPCA in survey mode and the narrowness in angular space of the relatively cold solar wind. The MS- $\text{He}^+$  perpendicular distribution extends to almost twice the velocity when compared to the corresponding distribution in the SW region. This extension indicates accelerated  $\text{He}^+$  PUIs, perpendicular to the magnetic field. In the MS- $\text{He}^+$  1-D distribution, the dotted gold and turquoise lines and the reflection ratio values are representative of our reflection analysis, discussed next.

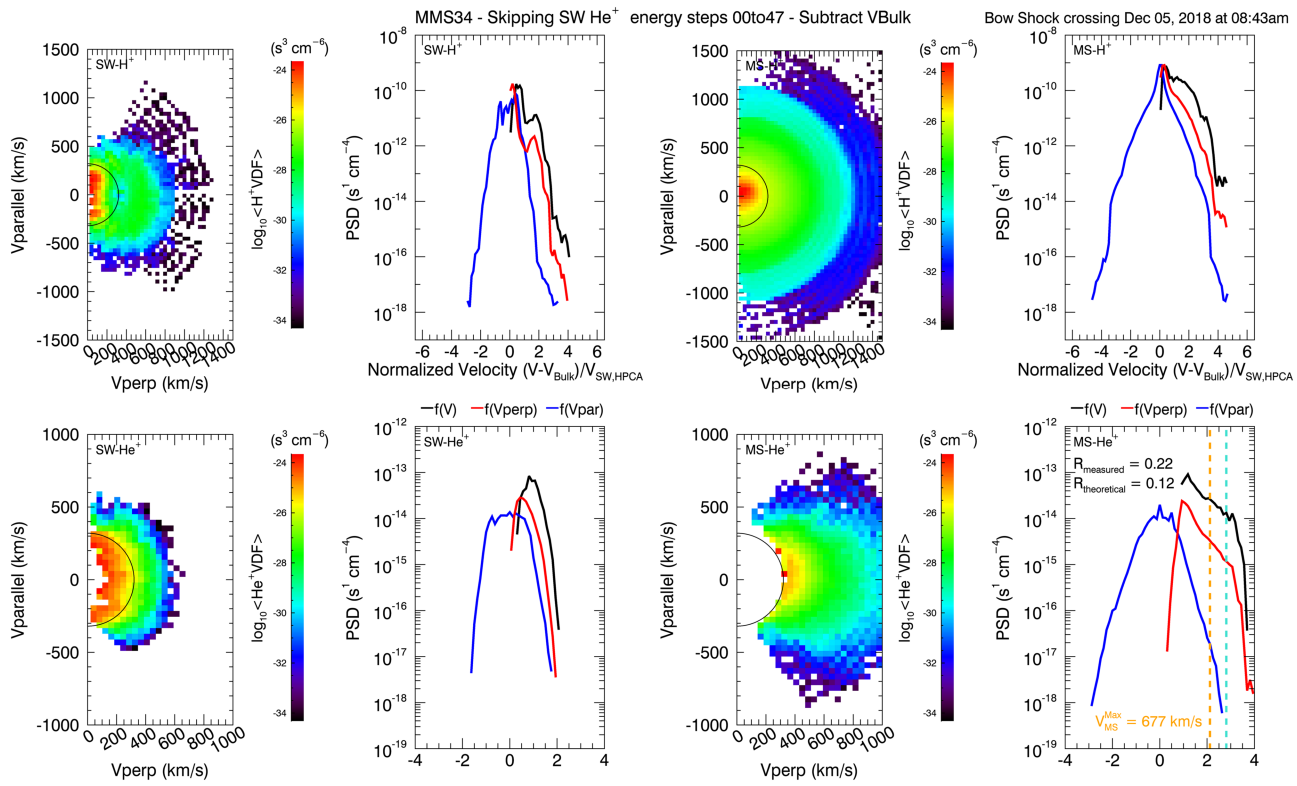


**Figure 2.** Phase space distributions for  $H^+$  and  $He^+$ , upstream (SW) and downstream (MS) of the shock. The top row corresponds to  $H^+$ , while the bottom row corresponds to  $He^+$ . The left two columns correspond to the SW interval, while the right two columns correspond to the MS interval. Each plot within the figure contains an interval-species label in the top left corner. Each 1-D distribution shows three curves:  $f(V)$  in black,  $f(V_{\text{perp}})$  in red, and  $f(V_{\text{par}}$ ) in blue. The black semi-circle in each 2-D distribution indicate the average value of  $V_{SW,HPCA}$  used to normalize the 1-D distributions. The gold dotted line in the MS- $He^+$  plot indicates the cutoff velocity  $V_{MS}^{Max}$  used to calculate the measured  $He^+$  reflection ratio, and the turquoise line represents the maximum energy gain of a  $He^+$  PUI due to a single reflection. The measured and theoretical reflection ratios are presented at the top of the MS- $He^+$  plot.

#### 4.1. Shock Reflection

We now seek to explain the signatures of accelerated downstream  $He^+$  ions, identified in Figure 2, by considering a simple model of singly reflected pickup  $He^+$ . This model and theoretical treatment is based largely on theory developed by Zank et al. (1996) and Lee et al. (1996). Upstream of the shock, if a SW PUI has a velocity component, normal to the shock that is too small to overcome the shock potential, then that PUI will be reflected. The reflected ion can then gyrate upstream and return to the shock, gaining energy due to the SW electric field. When viewed in the NIF, as outlined in Wilson et al. (2014), we assume that any portion of the distribution which has velocity less than that corresponding to the shock potential will reflect. The shock potential,  $\phi$ , is estimated (in the NIF frame) from the difference in energy of a bulk proton upstream and a bulk proton downstream of the shock:  $e\phi = \frac{1}{2}m_p(V_{SW,NIF}^2 - V_{MS,NIF}^2)$ . Due to bleed-over proton flux, HPCA underestimates the bulk proton velocity in the SW region. Thus, in our calculation of the shock potential we use the OMNI bulk solar wind velocity ( $\vec{V}_{SW,OMNI} = [-391, -30, -9]$  km/s), which is more representative of the solar wind vector upstream.

To model this event, we synthesize an initial 3-D upstream shell distribution, in the SW frame, given by

$$f(v) = \frac{n}{4\pi v^2} \frac{1}{2\pi^{1/2}\sigma} e^{-\frac{(v-v_0)^2}{2\sigma^2}}$$

where  $n$  is the ion density,  $v$  is the ion speed,  $v_0$  is the radius of the shell, and  $\sigma$  is the width of the shell (Zank et al., 1996). The density was  $n = 6 \times 10^{-6} \text{ cm}^{-3}$ , in order to match the peak density of our measured SW- $He^+$  distribution. Through comparison with the measured SW- $He^+$  distribution, we found that  $\sigma = 0.23V_{SW,OMNI}$

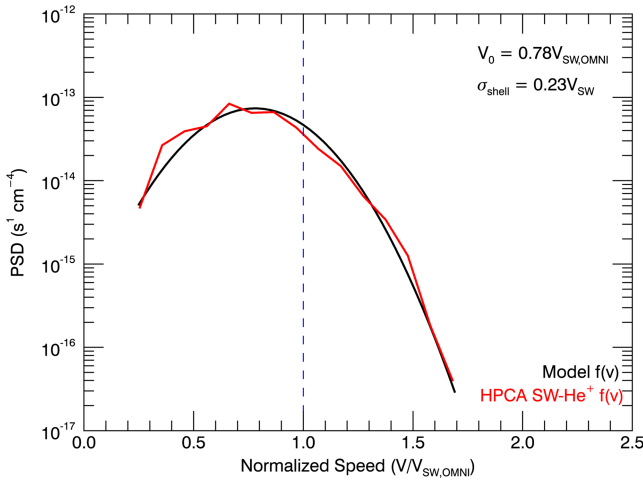


**Figure 3.** A comparison of the SW He<sup>+</sup> measured 1-D distribution (red) to the modeled upstream shell distribution. The blue dotted line represents V<sub>SW,OMNI</sub>.

potential,  $V_{reflect} = \sqrt{\frac{2}{m_{He}}} e\phi$ . This integrated value is then divided by the integral of the total distribution, resulting in  $R_{theoretical} = 0.12$ .

#### 4.2. Measured Reflection Ratio

In our analysis, distributions are viewed in the local plasma frame, relative to the bulk velocity. In the MS interval, the bulk proton speed is significantly smaller than that of the SW interval ( $V_{SW,HPCA} \sim 320$  km/s,  $V_{MS} \sim 83$  km/s) and the deflection of the bulk velocity vector is <5°. Thus, neglecting the shock potential, an ion's velocity in the SW frame can have a larger magnitude in the MS frame, simply due to the deceleration of the bulk solar wind. A transmitted PUI, without being accelerated by the shock, will lose energy  $e\phi$ . This distorts the shell distribution and decreases the maximum energy found in the MS. Due to the underestimate of the bulk solar wind speed by HPCA, we use the OMNI solar wind speed to constrain the speed of a He<sup>+</sup> PUI in the SW region. We assume that a He<sup>+</sup> PUI in the SW region has speed,  $V_{PUI} \leq 2V_{SW,OMNI}$ . The maximum energy of an upstream He<sup>+</sup> PUI in the spacecraft (SC) frame is then

$$E_{SC,up}^{Max} = 2m_{He}V_{SW,OMNI}^2$$

The maximum downstream energy is then

$$E_{SC,dn}^{Max} = E_{SC,up}^{Max} - e\phi$$

Lastly, the maximum speed of this He<sup>+</sup> PUI in the MS plasma frame is estimated by first converting  $E_{SC,dn}^{Max}$  to a He<sup>+</sup> ion speed and then subtracting the MS bulk plasma speed:

$$V_{MS}^{Max} = \sqrt{\frac{2}{m_{He}}} E_{SC,dn}^{Max} - V_{MS} \approx 677 \text{ km/s}$$

We assume that particles with speeds,  $V > V_{MS}^{Max}$ , have been accelerated by their interaction with the shock. In this estimate, we only consider the electrostatic force of the shock potential. Immediately downstream, ions that were barely able to overcome the shock potential will begin to gyrate about the MS magnetic field. This gyration can lead to energization by other mechanisms such as shock surfing (Lee et al., 1996). However, to include these finite gyroradius effects in our analysis would require a particle simulation, which is beyond the scope of this paper. Thus, it is likely that larger numbers of incident ions are initially reflected and so our measured reflection ratio acts as a lower limit to He<sup>+</sup> reflection. The percent of He<sup>+</sup> ions that are accelerated by the shock is then the ratio of psd corresponding to speeds above  $V_{MS}^{Max}$  to total psd. This accelerated ratio is shown on the MS-He<sup>+</sup> 1-D plot of Figure 2 and was calculated to be  $R_{measured} = 0.22$ . Note that due to our energy filtering of the He<sup>+</sup> distributions, part of the reflected portion of our measured 3-D VDFs is

and  $v_0 = 0.78V_{SW,OMNI}$  provided good agreement between the two. Figure 3 shows the measured SW-He<sup>+</sup> distribution from HPCA (red) and the integrated 1-D model distribution results for these parameters. The dotted blue line represents V<sub>SW,OMNI</sub>. From this figure, we deduce that the measured distribution agrees well with the modeled shell distribution. Owing to the peak radius of  $\sim 0.78 \bar{V}_{SW,OMNI}$ , it may be that the distribution has experienced some adiabatic cooling. However, a more likely explanation is to attribute this to the velocity of the neutral particle from which a PUI is formed. If the PUI is born with a radial velocity, acquired from the neutral population, then the resulting shell radius would be smaller than V<sub>SW</sub> (Möbius et al., 1999).

Lastly, we calculate a theoretical reflection ratio from the 3-D model distribution. The distribution is first translated into the NIF frame, preserving the radius of the shell and shifting its center to  $\bar{V}_{SW,NIF}$ . The reflected portion of the shell is then integrated by considering the portion of the distribution with normal velocities incident to the shock that are less than the velocity corresponding to the shock

removed. Thus, we are unable to directly calculate the  $\text{He}^+$  reflection ratio from the 3-D VDF. However, due to the shell-like appearance of the 2-D SW- $\text{He}^+$  distribution in Figure 2 and for simplicity, we assume that the upstream  $\text{He}^+$  distribution is isotropic in the plasma frame.

Comparing our theoretical and measured  $\text{He}^+$  reflection ratios, we observe a higher reflection ratio than expected. This may be due to the assumption of an isotropically filled shell distribution used in our theoretical model, or to the simplicity of our analysis in considering only the electrostatic force of the shock potential. We note, however, that our measured reflection ratio for  $\text{He}^+$ , which acts as a lower limit due to our consideration of only the electrostatic force acting on the ions, is much smaller than a result from Oka et al. (2002). In this paper, the authors simulated a GEOTAIL crossing of Earth's quasi-perpendicular ( $\theta_{Bn} = 76^\circ$ ) bow shock and reported a simulated  $\text{He}^+$  reflection ratio of  $\sim 51\%$ . This simulation included effects due to the IMF Lorentz force, in addition to effects due to the electrostatic shock potential. The Lorentz force helped to reflect PUIs that were not solely reflected by the shock potential, thus leading to a larger reflection ratio when compared to our work.

In order to gain insight into the contribution of other acceleration mechanisms, such as shock surfing, we estimated the maximum energy gain ( $\Delta\varepsilon$ ) of a singly reflected  $\text{He}^+$  PUI in the SW frame using results from Zank et al. (1996):

$$\Delta\varepsilon \leq 2m_p V_{SW,OMNI} V_{Spec}$$

Here  $V_{Spec}$  corresponds to the shock potential and is calculated from equation (8) of Zank et al. (1996) to be  $V_{Spec} = 132$  km/s. The velocity gain of a  $\text{He}^+$  PUI in the MS frame ( $\Delta v$ ) was found by solving

$$\Delta\varepsilon = \frac{1}{2} m_{He} \Delta v^2$$

This gave  $\Delta v \leq 221$  km/s =  $0.69V_{SW,HPCA}$ . The maximum speed at which we expect to observe singly reflected ions in the MS frame is then the sum of  $V_{MS}^{Max}$  and  $\Delta v^{Max} = 0.69V_{SW,HPCA}$ , and is plotted in the MS- $\text{He}^+$  panel of Figure 2 (turquoise line). The presence of higher-speed ions beyond this value suggests that other mechanisms may contribute to the accelerated population. However, a full investigation of these effects is outside the scope of this paper.

## 5. Summary and Conclusions

In this paper we analyzed MMS observations of a high Mach number perpendicular shock crossing at Earth's bow shock. We measured the distribution of pickup  $\text{He}^+$  in the upstream solar wind, and compared it to the accelerated population of  $\text{He}^+$  downstream of the shock. There appears to be pitch angle scattering beyond that expected for simple changes in the magnetic field direction during the averaging interval. Thus, in modeling the upstream  $\text{He}^+$  distribution, we found a shell distribution more appropriate than a torus or ring distribution. This observation of an apparently uniform PUI shell distribution and the implications for its formation out of a PUI ring beam requires further research.

By comparing measured ion reflection ratios to theoretically expected ratios and considering only single reflections, we conclude that the dominant acceleration process for PUI  $\text{He}^+$  at Earth's high Mach number and perpendicular bow shock is consistent with single reflection. Due to the simplistic nature of our analyses, our calculated ratio provides a lower limit for the ratio of accelerated  $\text{He}^+$ . In order to fully classify the role of shock reflection in accelerating PUIs, a similar analysis of quasi-perpendicular shocks with varying Mach number and geometry is needed. This may be achieved by analyzing shock crossings observed by MMS.

## Acknowledgments

This work is supported by NASA grant 80NSSC18K1366 and by MMS contract NNG04EB99C. The MMS data sets are accessible through the MMS Science Data Center website (<https://lasp.colorado.edu/mms/sdc/public/>). OMNI data were obtained from the GSFC/SPDF OMNIWeb website (<http://omniweb.gsfc.nasa.gov>).

## References

- Auer, P. L. (1971). Thermalization in the Earth's bow shock. *Journal of Geophysical Research*, 76(13), 2927–2939.
- Burch, J. L., Miller, G. P., De Los Santos, A., Pollock, C. J., Pope, S. E., Valek, P. W., & Young, D. T. (2005). Technique for increasing dynamic range of space-borne ion composition instruments. *The Review of Scientific Instruments*, 76(10), 103301. <https://doi.org/10.1063/1.2084867>
- Drews, C., Berger, L., Taut, A., Peleikis, T., & Wimmer-Schweingruber, R. F. (2015). 2D  $\text{He}^+$  pickup ion velocity distribution functions: STEREO PLASTIC observations. *Astronomy and Astrophysics*, 575, A97. <https://doi.org/10.1051/0004-6361/201425271>
- Drews, C., Berger, L., Wimmer-Schweingruber, R. F., & Galvin, A. B. (2013). Interstellar  $\text{He}^+$  ring-beam distributions: Observations and Implications. *Geophysical Research Letters*, 40, 1468–1473. <https://doi.org/10.1002/grl.50368>

- Ellison, D. C., Jones, F. C., & Baring, M. G. (1999). Direct acceleration of pickup ions at the solar wind termination shock: The production of anomalous cosmic rays. *The Astrophysical Journal*, 512(1), 403–416. <https://doi.org/10.1086/306739>
- Giacalone, J., & Jokipii, J. R. (1995). Simulations of pickup-ion acceleration at quasi-perpendicular shocks. *Space Science Reviews*, 72(1-2), 441–446. <https://doi.org/10.1007/BF00768818>
- Gloeckler, G., & Geiss, J. (1998). Interstellar and inner source pickup ions observed with Swics on Ulysses. *Space Science Reviews*, 86(1-4), 127–159. <https://doi.org/10.1023/A:1005019628054>
- Gloeckler, G., Geiss, J., & Fisk, L. A. (2004). Heating of pickup and solar wind ions at Jupiter's bow shock, AIP Conference Proceedings, 719, 201 (2004); <https://doi.org/10.1063/1.1809518>
- Gloeckler, G., Geiss, J., Roelof, E. C., Fisk, L. A., Ipavich, F. M., Ogilvie, K. W., et al. (1994). Acceleration of interstellar pickup ions in the disturbed solar wind observed on Ulysses. *Journal of Geophysical Research*, 99(A9), 17,637–17,643. <https://doi.org/10.1029/94JA01509>
- Gloeckler, G., Möbius, E., Geiss, J., Bzowski, M., Chalov, S., Fahr, H., et al. (2004). Observations of the helium focusing cone with pickup ions. *Astronomy and Astrophysics*, 426(3), 845–854. <https://doi.org/10.1051/0004-6361:20035768>
- Gloeckler, G., Schwadron, N. A., Fisk, L. A., & Geiss, J. (1995). Weak pitch angle scattering of few MV rigidity ions from measurements of anisotropies in the distribution function of interstellar pickup  $H^+$ . *Geophysical Research Letters*, 22(19), 2665–2668. <https://doi.org/10.1029/95GL02480>
- Gomez, R. G., Fuselier, S. A., Mukherjee, J., Gonzalez, C. A., Burch, J. L., Strangeway, R. J., & Starkey, M. J. (2019). The extra-magnetospheric ion environment as observed by the Magnetospheric Multiscale mission Hot Plasma Composition Analyzer (MMS-HPCA). *Journal of Geophysical Research: Space Physics*, 124, 1509–1524. <https://doi.org/10.1029/2018JA025392>
- Kucharek, H., Möbius, E., Li, W., Farrugia, C. J., Popecki, M. A., Galvin, A. B., et al. (2003). On the source and acceleration of energetic  $He^+$ : A long-term observation with ACE/SEPICA. *Journal of Geophysical Research*, 108(A10), 8040. <https://doi.org/10.1029/2003JA009938>
- Kucharek, H., & Scholer, M. (1995). Injection and acceleration of interstellar pickup ions at the heliospheric termination shock. *Journal of Geophysical Research*, 100(A2), 1745–1754. <https://doi.org/10.1029/94JA02559>
- Lee, M. A., Shapiro, V. D., & Sagdeev, R. Z. (1996). Pickup ion energization by shock surfing. *Journal of Geophysical Research*, 101(A3), 4777–4789. <https://doi.org/10.1029/95JA03570>
- Leroy, M. M., Goodrich, C. C., Winske, D., Wu, C. S., & Papadopoulos, K. (1981). Simulation of a perpendicular bow shock. *Geophysical Research Letters*, 8, 12, 1269–1272.
- McComas, D. J., Bzowski, M., Fuselier, S. A., Frisch, P. C., Galli, A., Izmodenov, V. V., et al. (2015). Local interstellar medium: Six years of direct sampling by IBEX. *The Astrophysical Journal Supplement Series*, 220(2), 22. <https://doi.org/10.1088/0067-0049/220/2/22>
- McComas, D. J., Sironstein, E. J., Bzowski, M., Elliott, H. A., Randol, B., Schwadron, N. A., et al. (2017). Instellar pickup ion observations to 38au. *The Astrophysical Journal Supplement Series*, 233(8), 14. <https://doi.org/10.3847/1538-4365/aa91d2>
- Merka, J., Szabo, A., Slavin, J. A., & Peredo, M. (2005). Three-dimensional position and shape of the bow shock and their variation with upstream Mach numbers and interplanetary magnetic field orientation. *Journal of Geophysical Research*, 110, A04202. <https://doi.org/10.1029/2004JA010944>
- Möbius, E., Bzowski, M., Chalov, S., Fahr, H. J., Gloeckler, G., Izmodenov, V., et al. (2004). Synopsis of the interstellar He parameters from combined neutral gas, pickup ion and UV scattering observations and related consequences. *Astronomy and Astrophysics*, 426(3), 897–907. <https://doi.org/10.1051/0004-6361:20035834>
- Möbius, E., & Hovestadt, D. (1985). Direct observations of  $He^+$  pick-up ions of interstellar origin in the solar wind. *Nature*, 318, 426 EP.
- Möbius, E., Litvinenko, Y., Grünwaldt, H., Aellig, M. R., Bogdanov, A., Ipavich, F. M., et al. (1999). Direct evidence of the interstellar gas flow velocity in the pickup ion cut-off as observed with SOHO CELIAS CTOF. *Geophysical Research Letters*, 26(20), 3181–3184. <https://doi.org/10.1029/1999GL003644>
- Möbius, E., Racinski, D., Lee, M. A., & Isenberg, P. A. (1998). Decreases in the antisunward flux of interstellar pickup  $He^+$  associated with radial interplanetary magnetic field. *Journal of Geophysical Research*, 103(A1), 257–265. <https://doi.org/10.1029/97JA02771>
- Oka, M., Terasawa, R., & Noda, H. (2002). Acceleration of interstellar helium pickup ions at the Earth's bow shock: GEOTAIL observation. *Geophysical Research Letters*, 29(14), 1688. <https://doi.org/10.1029/2001GL014150>
- Sckopke, N. (1995). Ion heating at the Earth's quasi-perpendicular bow shock. *Advances in Space Research*, 15(8/9), 261–269. [https://doi.org/10.1016/0273-1177\(94\)00106-B](https://doi.org/10.1016/0273-1177(94)00106-B)
- Sckopke, N., & Paschmann, G. (1983). Evolution of ion distributions across the nearly perpendicular bow shock: Specularly and non-specularly reflected-gyrating ions. *Journal of Geophysical Research*, 88(A8), 6121–6136. <https://doi.org/10.1029/JA088iA08p06121>
- Sckopke, N., Paschmann, G., Brinca, A. L., Carlson, C. W., & Luhr, H. (1990). Ion thermalization in quasi-perpendicular shocks involving reflected ions. *Journal of Geophysical Research*, 95(A5), 6337–6352. <https://doi.org/10.1029/JA095iA05p06337>
- Sonnerup, B. U. O. (1969). Acceleration of particles reflected at a shock front. *Journal of Geophysical Research*, 74(5), 1301–1304.
- Torbert, R., Russell, C. T., Magnes, W., Ergun, R. E., Lindqvist, P.-A., LeContel, O., et al. (2016). The FIELDS instrument suite on MMS: Scientific objectives, measurements, and data products. *Space Science Reviews*, 199(1–4), 105–135. <https://doi.org/10.1007/s11214-014-0109-8>
- Vallerga, J., Lallement, R., Lemoine, M., Dalaudier, F., & McMullin, D. (2004). EUVE observations of the helium glow: Interstellar and solar parameters. *Astronomy and Astrophysics*, 426(3), 855–865. <https://doi.org/10.1051/0004-6361:20035887>
- Vasyliunas, V. M., & Siscoe, G. L. (1976). On the flux and the energy spectrum of interstellar ions in the solar system. *Journal of Geophysical Research*, 81(7), 1247–1252. <https://doi.org/10.1029/JA081i007p01247>
- Wilson, L. B. III, Sibeck, D. G., Breneman, A. W., Le Contel, O., Cully, C., Turner, D. L., et al. (2014). Quantified energy dissipation rates in the terrestrial bow shock: 1. Analysis techniques and methodology. *Journal of Geophysical Research: Space Physics*, 119, 6455–6474. <https://doi.org/10.1002/2014JA019929>
- Witte, M. (2004). Kinetic parameters of interstellar neutral helium. *Astronomy and Astrophysics*, 426(3), 835–844. <https://doi.org/10.1051/0004-6361:20035956>
- Young, D. T., Burch, J. L., Gomez, R. G., De Los Santos, A., Miller, G. P., Wilson, P. IV, et al. (2014). Hot Plasma Composition Analyzer for the Magnetospheric Multiscale mission. *Space Science Reviews*, 199(1–4), 407–470. <https://doi.org/10.1007/s11214-014-0119-6>
- Zank, G. P., Pauls, H. L., Cairns, I. H., & Webb, G. M. (1996). Interstellar pickup ions and quasi-perpendicular shocks: Implications for the termination shock and interplanetary shocks. *Journal of Geophysical Research*, 101(A1), 457–477. <https://doi.org/10.1029/95JA02860>
- Zirnstein, E. J., McComas, D. J., Kumar, R., Elliott, H. A., Szalay, J. R., Olkin, C. B., et al. (2018). In situ observations of preferential pickup ion heating at an interplanetary shock. *Physical Review Letters*, 121(7), 075102. <https://doi.org/10.1103/PhysRevLett.121.075102>